Research Square

Preprints are preliminary reports that have not undergone peer review.
They should not be considered conclusive, used to inform clinical practice,
or referenced by the media as validated information.

Dynamic helical poly[4]helicene nanoribbon

Tomoyuki Ikai

ikai@chembio.nagoya-u.ac.jp

Nagoya University https://orcid.org/0000-0002-5211-2421

Hayato Inagaki

Nagoya University

Kosuke Oki

Seikei University

Masaya Yoshida

Nagoya University

Jenny Pirillo

Nagoya University

Yuh Hijikata

Nagoya University https://orcid.org/0000-0003-4883-5085

Eiji Yashima

National Tsing Hua University

Article

Keywords:

Posted Date: October 13th, 2025

DOI: https://doi.org/10.21203/rs.3.rs-7760059/v1

License: This work is licensed under a Creative Commons Attribution 4.0 International License.
Read Full License

Additional Declarations: There is **NO** Competing Interest.

Version of Record: A version of this preprint was published at Nature Communications on August 15th, 2026. See the published version at https://doi.org/10.1038/s41467-026-76724-9.

Dynamic helical poly[4]helicene nanoribbon

Tomoyuki Ikai,[1,2,*] Hayato Inagaki,[1] Kosuke Oki,[1,3] Masaya Yoshida,[1] Jenny Pirillo,[4] Yuh Hijikata,[5] and Eiji Yashima[1,6,*]

[1] Department of Molecular and Macromolecular Chemistry, Graduate School of Engineering, Nagoya University, Chikusa-ku, Nagoya 464-8603, Japan

[2] Precursory Research for Embryonic Science and Technology (PRESTO), Japan Science and Technology Agency (JST), Kawaguchi, Saitama 332-0012, Japan

[3] Present address: Faculty of Science and Technology, Seikei University, Musashino, Tokyo 180-8633, Japan

[4] Department of Materials Chemistry, Graduate School of Engineering, Nagoya University, Chikusa-ku, Nagoya 464-8603, Japan

[5] Research Center for Net Zero Carbon Society, Institute of Innovation for Future Society, Nagoya University, Chikusa-ku, Nagoya 464-8601, Japan

[6] Present address: Department of Chemical Engineering, National Tsing Hua University, 101, Sec. 2, Kuang-Fu Road, Hsinchu, 30013, Taiwan, R.O.C.

* Correspondence: ikai@chembio.nagoya-u.ac.jp; yashima@chembio.nagoya-u.ac.jp

Abstract

The precise synthesis of helical graphene nanoribbons (GNRs) with a controlled handedness has a transformative potential as the promising chiral carbon materials. We now report the first synthesis of a dynamic helical poly[4]helicene nanoribbon, a novel class of helical GNRs, entirely composed of configurationally labile [4]helicene subunits, which has been achieved through the quantitative intramolecular multifold cyclization of the nonhelical precursor polymer. The [4]helicene repeating units of the poly[4]helicene nanoribbon are mechanically coupled to each other, providing an equal mixture of an interconvertible long sequence of right (*P*)- and left (*M*)-handed helical [4]helicene subunits. Therefore, in an optically-active solvent, a fully (*P*)- or (*M*)-helical poly[4]helicene nanoribbon consisting of homochiral (*P*)- or (*M*)-[4]helicene subunits can be induced in a highly-cooperative manner, showing a right- or left-handed circularly polarized luminescence, respectively, which can be switched.

Polycyclic aromatic hydrocarbons (PAHs) are at the heart of materials science and serve as a critical component of advanced functional materials. Despite the simple elemental composition of carbon and hydrogen, their photophysical and electrochemical properties are highly dependent on the fusion mode and the geometries (e.g., planar and nonplanar).[1-4] [*n*]Helicenes are a typical class of nonplanar PAHs with a spiral-shaped π-conjugated framework consisting of more than four ($n \geq 4$) *ortho*-fused benzene rings.[5-8] In particular, higher [*n*]helicenes ($n \geq 6$) and their analogues are configurationally stable in solution due to steric overcrowding between the terminal benzene rings, which creates sufficiently high helix-inversion barriers (> 35 kcal/mol).[9,10] To date, the isolated left (*M*)- and right (*P*)-handed helical isomers of higher [*n*]helicenes have been applied to chiral materials with a long-term stability for circularly polarized luminescence (CPL),[11] non-linear optics,[8] spin filtering,[12] and chiral ligands for asymmetric catalysis.[13] On the other hand, the smallest helicene, [4]helicene, has a rather low helix-inversion barrier of ca. 4 kcal/mol and exists in rapid equilibrium between the (*M*)- and (*P*)-forms in solution.[14] [4]Helicene and its analogues have been crucial in the fundamental study of stereochemical dynamics,[10] but have been excluded as a structural motif from the creation of chiral materials due to their kinetically labile helical conformation.

Graphene nanoribbons (GNRs) with a quasi-one-dimensional elongated PAH structure are an emerging member of the graphene family. Over the past few decades, GNRs have attracted increasing interest for potential applications in nanoelectronics and spintronics due to their unique optical, electronic, and magnetic properties, which can be finely tuned through width control and edge engineering.[15-18] In addition, recent efforts have concentrated on incorporating non-planarity into the GNRs, because such non-planar GNRs not only enhance solubility and solution processability but also offer new chemical and physical aspects that are absent in their planar counterparts, thereby providing an untapped potential in GNR applications.[1,19,20] A typical approach to induce curvature and distortion in GNRs involves the incorporation of [4]- and [5]helicene subunits at the periphery of the graphene structures, forming nonplanar cove-[21-24] and fjord-edges,[25-27] respectively (Fig. 1a). Recently, a preferred-handed helix induction in the multiple helicene units embedded in the cove-edged nanographene molecules[28-30] and fjord-edged GNRs[31] has been achieved through the covalent-bond driven chirality transfer from the optically-active components, such as [6]helicene, binaphthyl, and 1-

phenylethyl units, incorporated into the GNR framework. However, there is no precedent for the dynamic control of the GNR helicity through supramolecular chiral interactions.

We recently reported a highly versatile acid-promoted alkyne benzannulation, applicable to quantitative and chemoselective intramolecular multifold cyclizations.[32-34] Its broad substrate applicability enabled the synthesis of a variety of defect-free ladder-type molecules and polymers, including classical[35] and expanded[36] helicenes, one-handed helical ladder polymers[37-39] (e.g., poly-(*S*)-**A**[38] in Fig. 1b), and fully π-conjugated coplanar ladder polymers (e.g., poly-**B**).[34] We envisioned that our developed defect-free synthetic method could be applied to a dynamic helical GNR, a class of unique fully-fused aromatic helical ladder polymers, by incorporating dynamic helical [4]helicene subunits into the fully π-conjugated GNR backbones.

We now report the unprecedented defect-free synthesis of a novel dynamic helical poly[4]helicene nanoribbon, a novel class of helical GNRs,[40] entirely composed of the configurationally labile [4]helicene subunits through acid-promoted alkyne benzannulations (Fig. 1c) and further a right (*P*)- or left (*M*)-handed helicity induction in the poly[4]helicene nanoribbon backbone through supramolecular chirality transfer from naturally-occurring optically-active solvents (Fig. 1d),[41-43] in which the kinetically labile [4]helicene subunits also possess the corresponding homochiral (*P*)- or (*M*)-helicity, respectively, in a highly-cooperative manner. We note that little or no excess one-handed helicity could be induced in the corresponding [4]helicene oligomers and precursor linear polymer, highlighting the indispensable role of the cooperative chiral interactions of adjacent dynamic helical [4]helicene subunits that are mechanically coupled to the helicity of the poly[4]helicene nanoribbon as supported by molecular dynamics (MD) simulation.

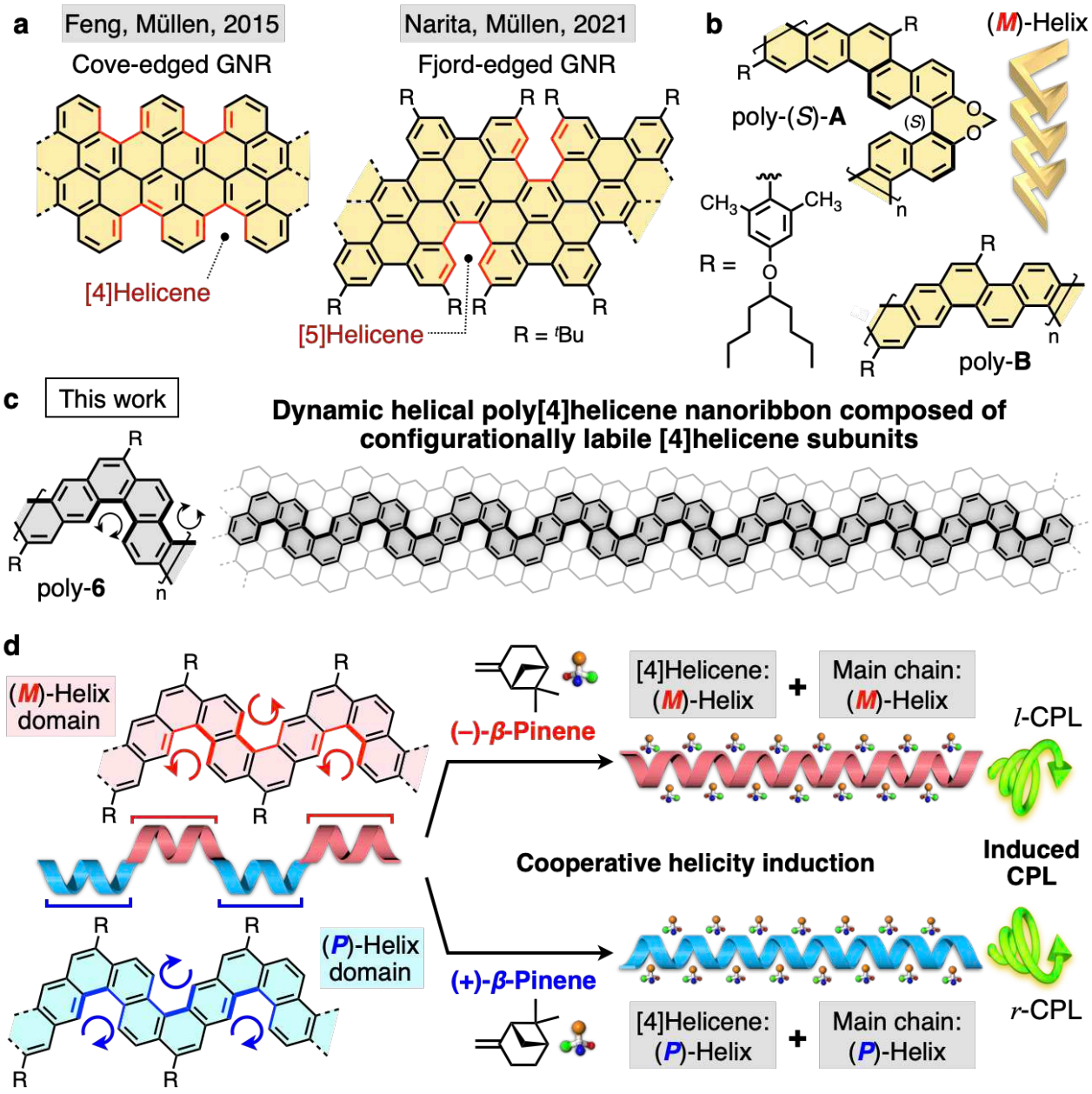


Fig. 1 | Development of a dynamic helical poly[4]helicene nanoribbon composed of configurationally labile [4]helicene subunits. a, Representative examples of the partial structures of the cove- and fjord-edged graphene nanoribbons (GNRs) incorporating the [4]- and [5]helicene subunits at the graphene periphery, respectively. **b**, Structures of a one-handed helical ladder polymer (poly-(*S*)-**A**) and a fully π-conjugated coplanar ladder polymer (poly-**B**). **c**, Structure of a dynamic helical poly[4]helicene nanoribbon (poly-**6**) composed entirely of configurationally labile [4]helicene subunits. **d**, Schematic illustrations of cooperative one-handed helicity induction in the poly[4]helicene nanoribbon mediated by deracemization of the dynamically racemic [4]helicene repeating units through supramolecular chirality transfer from optically-active natural solvents ((–)- and (+)-*β*-pinene), resulting in circularly polarized luminescence (CPL) capable of switching the polarization handedness (left (*l*) and right (*r*)).

Results and discussion

Synthesis of dynamic helical poly[4]helicene nanoribbon composed of configurationally labile [4]helicene subunits

We first investigated the quantitative synthesis of the double and quadruple [4]helicene oligomers (double-**2** and quadruple-**4**) composed of 7 and 12 fused benzene rings, respectively, as oligomer models of the poly[4]helicene nanoribbon (Fig. 2a). The naphthalene-embedded cyclization precursors (**1** and **3**) containing two and four 2-(4-butoxy-2,6-dimethylphenyl)ethynyl pendants, respectively, were synthesized according to Supplementary Scheme 1. **1** and **3** would be equilibrium mixtures of two and six interconvertible diastereomers, respectively, due to the dynamic nature of the multiple biaryl axial chiralities,[36] as confirmed by their variable-temperature ^{1}H NMR analysis (Supplementary Figs. 2 and 3). The trifluoroacetic acid (TFA)-promoted alkyne benzannulations of **1** and **3** exclusively proceeded at the 2- and/or 6-positions of the naphthalene rings without any side reactions, affording double-**2** and quadruple-**4** in quantitative yields, respectively, as revealed by 1D and 2D NMR (Fig. 2b and Supplementary Figs. 4–7), IR (Supplementary Fig. 8a–d), and high-resolution mass (see Supplementary section 2) spectral analyses. The double [4]helicene structure of the double-**2** was further unambiguously determined by single-crystal X-ray diffraction analysis (Fig. 2c and Supplementary Fig. 1), which revealed that double-**2** exists as a homochiral (*P*,*P*)- and (*M*,*M*)-enantiomeric pair in the crystal packing (Fig. 2d).

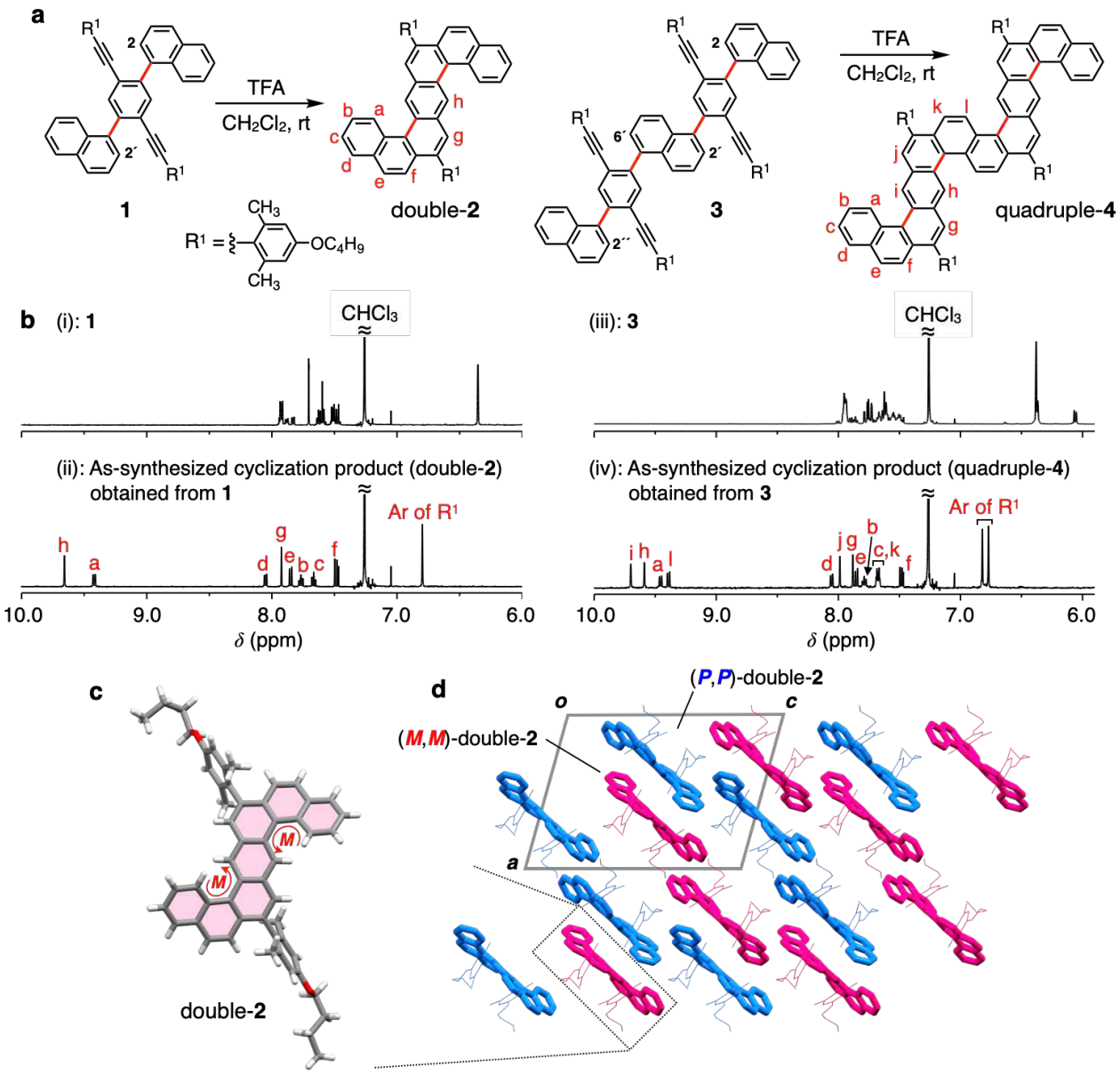


Fig. 2 | Quantitative and chemoselective synthesis of consecutively fused multiple [4]helicenes. a, Synthesis of consecutively fused multiple [4]helicenes (double-**2** and quadruple-**4**) through quantitative and chemoselective acid-promoted alkyne benzannulations of **1** and **3**, respectively. **b**, ^{1}H NMR spectra (500 MHz, $CDCl_3$, 25 °C) of **1** (i), **3** (iii), and as-synthesized cyclization products (double-**2** (ii) and quadruple-**4** (iv)) obtained from **1** and **3**, respectively. For the signal assignments and the corresponding IR spectra, see Supplementary Figs. 5, 7, and 8. **c**, X-ray crystal structure of double-**2**. **d**, Crystal packing structure of (*M*,*M*)/(*P*,*P*)-double-**2** as viewed along the *b* axis of the unit cell shown in gray. The helicene backbones and the 4-butoxy-2,6-dimethylphenyl pendant groups are represented by capped-stick and wireframe models, respectively, and (*M*,*M*)- and (*P*,*P*)-double-**2** are colored in red and blue, respectively. All the hydrogen atoms are omitted for clarity.

Following the success of the defect-free quantitative synthesis of multiple [4]helicene skeletons, we then synthesized the corresponding poly[4]helicene nanoribbon, in which the configurationally labile [4]helicene subunits are consecutively fused together by sharing the benzene and naphthalene units (Figs. 1c and 3a). Poly-**5** composed of alternating 1,5-linked-naphthalene and 2,5-diethynyl-substituted *p*-phenylene units was designed as a precursor polymer and synthesized by the Suzuki–Miyaura coupling copolymerization of the dibromo (**Ph**$_{\mathbf{Br}}$) and diboronic acid ester (**NAP**$_{\mathbf{Bpin}}$) monomers, followed by size-exclusion chromatography (SEC) fractionation (Supplementary Scheme 2). The number-average molar mass (M_n) and degree of polymerization (DP_n) of poly-**5** were estimated to be 2.65×10^4 and 36, respectively, by SEC (Fig. 3a and Supplementary Table 1). Poly-**5** was then converted to the poly[4]helicene nanoribbon (poly-**6**) by alkyne benzannulations (Fig. 3a and Supplementary Scheme 3) during which the alkyne groups in poly-**5** were completely consumed as confirmed by IR analysis (Supplementary Fig. 8e,f), while virtually retaining the M_n value (2.52×10^4). The lower-molar-mass poly[4]helicene (poly-**6**-8.5K) with an M_n value of 0.85×10^4 was also synthesized from the corresponding precursor (poly-**5**-8.9K) to investigate the molar mass effect (see below and Supplementary Schemes 2 and 3).

The matrix-assisted laser desorption-ionization time-of-flight mass (MALDI-TOF-MS) spectrum of poly-**6** showed main series of peaks with a regular interval of approximately 743 (*m*/*z*) mass, corresponding to the molar mass of the repeating [4]helicene unit (Supplementary Fig. 9). Poly-**6** showed broad, but distinct five aromatic proton resonances (H_a–H_e) in the ^{1}H NMR spectrum (Fig. 3b(ii) and Supplementary Fig. 10), which were fully assigned by 2D NMR (Supplementary Fig. 11). The H_a and H_d protons of the poly-**6** backbone showed remarkable downfield shifts compared to those of poly-**5** (Fig. 3b(i) and Supplementary Figs. 12 and 13) probably due to the strong ring current effect in the cove regions of the [4]helicene moieties, as observed in the oligomer models (double-**2** and quadruple-**4**) (Fig. 2b). These spectral data support the chemoselective formation of the poly[4]helicene. The absorption and photoluminescence (PL) spectra in chloroform are red-shifted in the order of double-**2** < quadruple-**4** < poly-**6** as anticipated (Fig. 3c). Double-**2**, quadruple-**4**, and poly-**6** showed a blue, light blue, and green fluorescence emission in chloroform under irradiation at 365 nm, and their quantum yields (Φ_F) were determined to be 13, 12, and 33%, respectively (Fig. 3d).

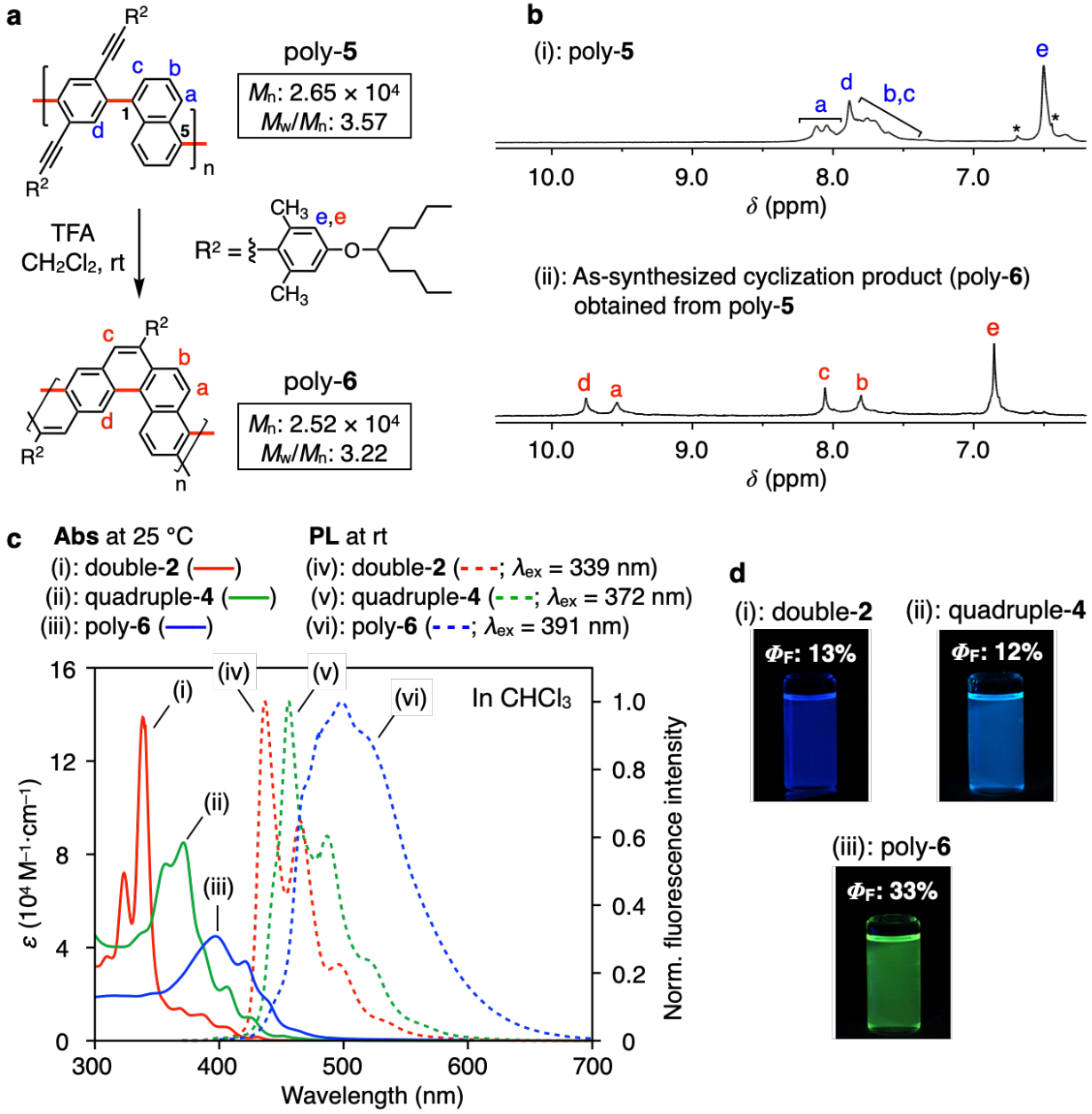


Fig. 3 | Defect-free synthesis of poly[4]helicene nanoribbon. a, Synthesis of a dynamic helical poly[4]helicene nanoribbon (poly-**6**) by quantitative and chemoselective acid-promoted alkyne benzannulations of poly-**5**. **b**, ^{1}H NMR spectra (500 MHz, 1,1,2,2-tetrachloroethane-d_2, 95 °C) of poly-**5** (i) and poly-**6** (ii). For the corresponding IR spectra, the variable-temperature ^{1}H NMR spectra, and the signal assignments, see Supplementary Figs. 8 and 10–13. Asterisks in (i) denote the aromatic protons from alkoxyphenyl pendants (R^2) at the terminal end (Supplementary Figs. 14 and 15). **c**, Absorption (solid lines) and normalized PL (dotted lines) spectra of double-**2** (i,iv), quadruple-**4** (ii,v), and poly-**6** (iii,vi) in chloroform at 25 °C (i–iii) and room temperature (iv–vi). [**2**, **4**, or poly-**6**] = 0.15 mM. **d**, Photographs of double-**2** (i), quadruple-**4** (ii), and poly-**6** (iii) in chloroform with 365-nm irradiation. Fluorescence quantum yields (Φ_F) are also shown.

Computational study of the poly[4]helicene nanoribbon

The poly[4]helicene nanoribbon (poly-**6**) formed with the fused benzene rings of dynamic helical [4]helicene subunits has the potential to form an equal mixture of an interconvertible long sequence of (*P*)- and (*M*)-handed helical [4]helicene units with rarely occurring helical reversals, as a result of the long-range cooperativity of the adjacent [4]helicene subunits. MD simulations were then performed with the 16-mer model of poly-**6** (hexadeca-**6**-H in Fig. 4a(i)) containing 32 alternating (*P*)- and (*M*)-handed helical [4]helicene subunits as an initial structure at 20 °C (293 K) (see Supplementary Video 1 and Supplementary Section 4). During the simulation, the helix-inversion sporadically occurred at various locations along the polymer chain, forming (*P*)- and (*M*)-helical domains with a consecutive sequence of up to five homochiral [4]helicene units (Fig. 4a(ii) and Supplementary Figs. 16 and 17). After 60 ns, the polymer chain was composed entirely of (*P*)- and (*M*)-helical domains separated by helix reversal points, except for a single isolated (*M*)-[4]helicene unit (Fig. 4a(ii) and Supplementary Fig. 16). The homochiral domain formation was accelerated at 400 K (Supplementary Video 2), where the isolated (*P*)- and (*M*)-[4]helicene units disappeared within ca. 20 ns and the number of the consecutive homochiral [4]helicene units in the domain reached nine (Supplementary Figs. 18 and 19). During the simulation period, only one or two helix-inversions were observed in the homochiral domains at 293 and 400 K, respectively, all of which occurred at the domain ends, but not within the domains (green squares in Supplementary Figs. 16 and 18). These results indicated that the homochiral sequence is energetically more stable than the heterochiral sequence containing helix reversals. In fact, the homochiral 4-mer oligomer model of poly-**6** (tetra-**6**), composed of eight (*M*)-[4]helicene units, is the most stable among the tested diastereomers that included one to four opposite-handed helical (*P*)-[4]helicene sequences with more than one helix reversal, as revealed by the density functional theory (DFT) calculations (Fig. 4b).[36] The excess free energy per helix reversal (helix reversal penalty) was estimated to be ca. 7–10 kJ/mol (Fig. 4b). These theoretical studies suggested that poly-**6** in chloroform appears to consist of relatively long (*P*)- and (*M*)-helical sequences separated by helix reversals with only a minimal presence of the unfavorable isolated opposite-handed helical [4]helicene unit (Fig. 4a(ii) and Supplementary Fig. 18b(ii)).

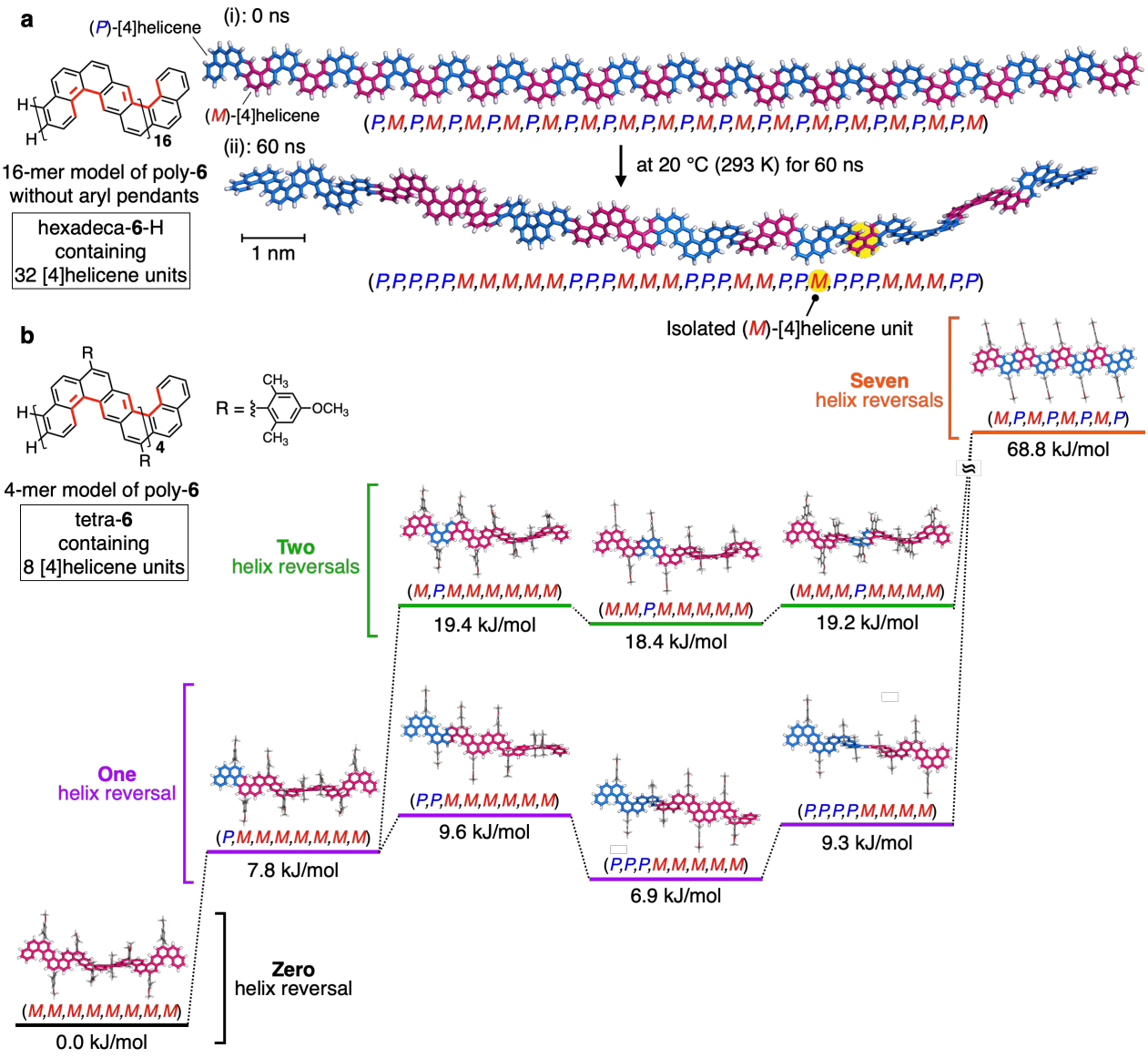


Fig. 4 | Computational structural analysis of poly[4]helicene nanoribbon. a, Side views of hexadeca-**6**-H (16-mer model of poly-**6** without aryl pendants) containing 32 [4]helicene units before (i) and after (ii) the molecular dynamics (MD) simulation at 20 °C (293 K) for 60 ns. The structures are represented by capped-stick models, and the carbon atoms of the (*P*)- and (*M*)-[4]helicene units in the backbone are highlighted in blue and red, respectively, for clarity. **b**, Relative free energies (kJ/mol) for tetra-**6** (4-mer model of poly-**6**) containing 8 [4]helicene units calculated by density functional theory (DFT) at the B3LYP/6-31G(d) level. For simplicity, the branched alkoxy pendants are replaced with methoxy groups.

Cooperative helicity induction in poly[4]helicene nanoribbon

Poly-**6** showed a clear induced circular dichroism (ICD) in the π-conjugated main-chain absorption region (300–470 nm) in chiral solvent/chloroform mixtures (80/20, v/v) at 25 °C (Fig. 5a(vi) and Supplementary Fig. 20a(i,ii,iv)). Among the investigated chiral solvents, (–)-*β*-pinene induced the most intense ICD in poly-**6** (Supplementary Fig. 20). The absorption and ICD intensity of a solution of poly-**6** in (–)-*β*-pinene/chloroform (80/20, v/v) at 25 °C remained unchanged after the solution was diluted 10-fold (Supplementary Fig. 21(ii)) or passed through a membrane filter (pore size: 0.22 μm) (Supplementary Fig. 21(iii)), indicating that the formation of aggregates in the presence of a chiral poor cosolvent could be excluded.[44-47] Therefore, the observed ICD can be most likely ascribed to the excess one-handed helix formation of poly-**6** (*P*- or *M*-rich) in the molecularly-dispersed state in response to the chirality of optically-active solvents,[41-43] as a result of the induction of the *P*- or *M*-helicity in each dynamic [4]helicene subunit that takes places in a highly-cooperative manner (Fig. 1d).

The nonhelical precursor polymer (poly-**5**) and the previously reported structural isomer (poly-**B** in Fig. 1b) of poly-**6**,[34] both of which lack a [4]helicene moiety in their backbone, showed no ICD in the presence of (–)-*β*-pinene (≥ 80 vol%) (Supplementary Fig. 22(i,iii)). This further supports the indispensable role of the consecutively fused dynamic helical [4]helicene sequence for the helicity induction in the poly-**6** backbone. The observed ICD pattern of poly-**6** in the presence of (–)-*β*-pinene was roughly identical to the theoretical CD pattern estimated by the time-dependent-DFT (TD-DFT) calculations of an (*M*)-handed helical 5-mer model of poly-**6** totally consisting of (*M*)-[4]helicene repeating units (Supplementary Fig. 23). Hence, the helical sense of poly-**6** as well as those of the corresponding [4]helicene subunits induced in (–)-*β*-pinene was assigned to the (*M*)-helix.

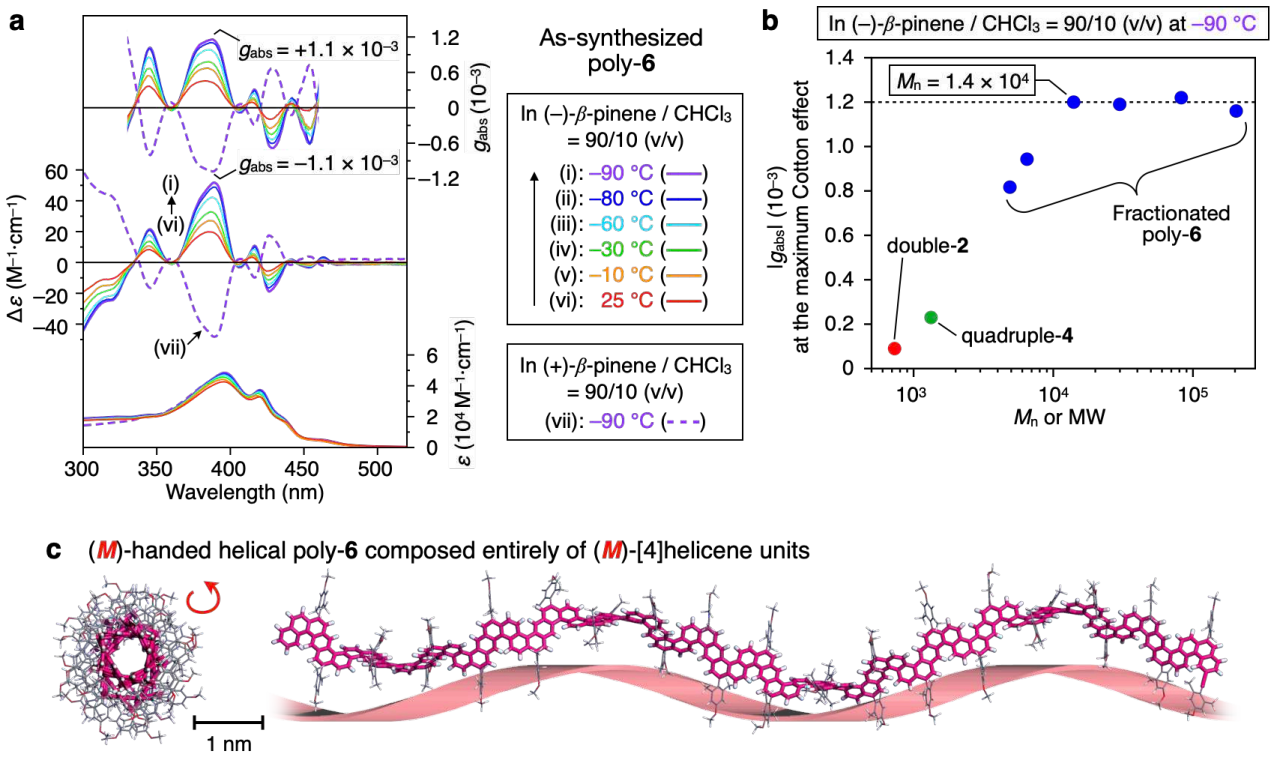


Fig. 5 | Cooperative one-handed helicity induction in poly[4]helicene nanoribbon. a, CD and absorption spectra of as-synthesized poly-**6** in (–)-*β*-pinene/chloroform (90/10, v/v) at different temperatures (–90 (i), –80 (ii), –60 (iii), –30 (iv), –10 (v), and 25 (vi) °C) and in (+)-*β*-pinene/chloroform (90/10, v/v) at –90 °C (vii). [Polymer] = 0.15 mM. **b**, Plots of Kuhn's dissymmetry factors ($|g_{abs}|$) at the maximum Cotton effect of fractionated poly-**6**, quadruple-**4**, and double-**2** versus the M_n (for poly-**6**) or molecular weights (MW) (for quadruple-**4** and double-**2**) value. For the SEC fractionation of as-synthesized poly-**6** and poly-**6**-8.5K and the corresponding CD spectra, see Supplementary Fig. 25. **c**, Top (left) and side (right) views of the geometry-optimized structures of the (*M*)-handed helical poly-**6** composed entirely of (*M*)-[4]helicene units with 16 repeating units obtained by the molecular mechanics (MM) calculations (Compass II force field). For simplicity, all alkoxy pendants are replaced with methoxy groups. The structures of the helical ladder backbones and alkoxyphenyl pendants are represented by capped-stick and wireframe models, respectively, and the carbon atoms of the helical ladder backbones are highlighted in red for clarity.

The ICD intensity of poly-**6** increased with the increasing (–)-*β*-pinene content (Supplementary Fig. 24) and decreasing temperature (Fig. 5a(i–vi)), reaching the Kuhn's dissymmetry factor (g_{abs} = $\Delta\varepsilon/\varepsilon$) of up to +1.1 × 10^{-3} in (–)-*β*-pinene/chloroform (90/10, v/v) at –90 °C (Fig. 5a(i)), indicating the dynamic nature of poly-**6**. Poly-**6** showed a mirror-image ICD (g_{abs} = –1.1 × 10^{-3}) when an enantiomeric (+)-*β*-pinene was used as a chiral cosolvent (Fig. 5a(vii)). Considering that the g_{abs} values of the previously reported fully one-handed helical conjugated polymers, including polyacetylenes, polyisocyanides, and poly(quinoxaline-2,3-diyl)s, are typically on the order of 10^{-3},[44,48] the helical sense excess of the [4]helicene subunits in the poly-**6** backbone is expected to be substantially biased toward the (*M*)-helicity in (–)-*β*-pinene/chloroform (90/10, v/v) at –90 °C (Fig. 5a(i)). Assuming the repeating [4]helicene units are fully deracemized by (–)-*β*-pinene, poly-**6** possesses not only the (*M*)-helicity of the repeating subunit, but also the main-chain (*M*)-helicity of the polymer backbone, resulting in a unique (*M*)-handed helical poly[4]helicene framework, entirely composed of consecutively fused all-(*M*) [4]helicene subunits (Fig. 5c).

The g_{abs} value at the maximum Cotton effect (around 382–389 nm) of poly-**6** in (–)-*β*-pinene/chloroform (90/10, v/v) at –90 °C increased with an increase in the molar mass (Fig. 5b and Supplementary Fig. 25) and reached an almost saturated value of 1.2 × 10^{-3} at the M_n value of more than 1.4 × 10^4 (corresponding to approximately >19 repeating units) (Fig. 5b). In addition, the oligomer models, double-**2** and quadruple-**4**, with molecular weights (MW) of 731 and 1334, respectively, showed very weak ICD signals ($|g_{abs}| \leq 0.2 \times 10^{-3}$) under the same conditions (Supplementary Fig. 25d(vii,viii)). These results suggest that the helicity induction in poly-**6** is significantly facilitated in the high molar-mass poly[4]helicene nanoribbon, in which a highly-cooperative effect could operate.

The (*M*)-helical domain, composed of (*M*)-[4]helicene subunits, appears to be significantly stabilized by (–)-*β*-pinene due to chiral solvation. This is in contrast to the opposite (*P*)-helical domain, which undergoes *P*-to-*M*-helix inversion (deracemization) of the [4]helicene subunits in response to the chirality of (–)-*β*-pinene. This helix-inversion process elongates the (*M*)-helical domain within the poly-**6** backbone. More specifically, in (–)-*β*-pinene/chloroform (90/10, v/v) at –90 °C, the homochiral (*M*)-[4]helicene units would elongate almost entirely along the polymer backbone, thereby forming a one-handed helical conformation throughout the polymer backbone (Fig. 5c). The dynamically

racemic helical [4]helicene repeating units of poly-**6** are fully mechanically coupled along the entire π-conjugated poly[4]helicene backbone. Therefore, chiral solvation, although its chiral bias seems to be very weak,[49] can be significantly amplified, resulting in the formation of an almost one-handed helical poly[4]helicene through highly enantioselective deracemization of the racemic [4]helicene subunits assisted by a chiral cosolvent. The present amplification of asymmetry substantially differs from the previously reported observation in dynamic helical copolymers and supramolecular helical assemblies composed of chiral/achiral and nonracemic monomers.[44,48] Notably, a one-handed helical poly[4]helicene nanoribbon is formed by the deracemization of dynamically racemic repeating monomer units within the polymer backbone due to chiral solvation. To the best of our knowledge, this is the first example of an excess one-handed helicity induction in GNRs by noncovalent chiral interactions.

Induced circularly polarized luminescence

Poly-**6** showed an intense CPL with a luminescence dissymmetry factor ($|g_{lum}|$) reaching 2.8×10^{-3} in (–)- or (+)-*β*-pinene/chloroform (90/10, v/v) at –90 °C (Fig. 6), which is the highest level reported for one-handed helical ladder polymers, including poly-(*S*)-**A**, composed of "optically-pure" monomer units (Fig. 1b).[34,37-39] This result further supports the nearly perfect degree of one-handed helicity induction in the [4]helicene subunits of poly-**6**, and consequently, the helicity of the polymer backbone. In response to the chirality of *β*-pinene, the handedness of poly-**6** can be switched, thus providing a unique switchable GNR that can produce both the left- and right-handed CPLs from a single material (Figs. 1d and 6(i,vi)).

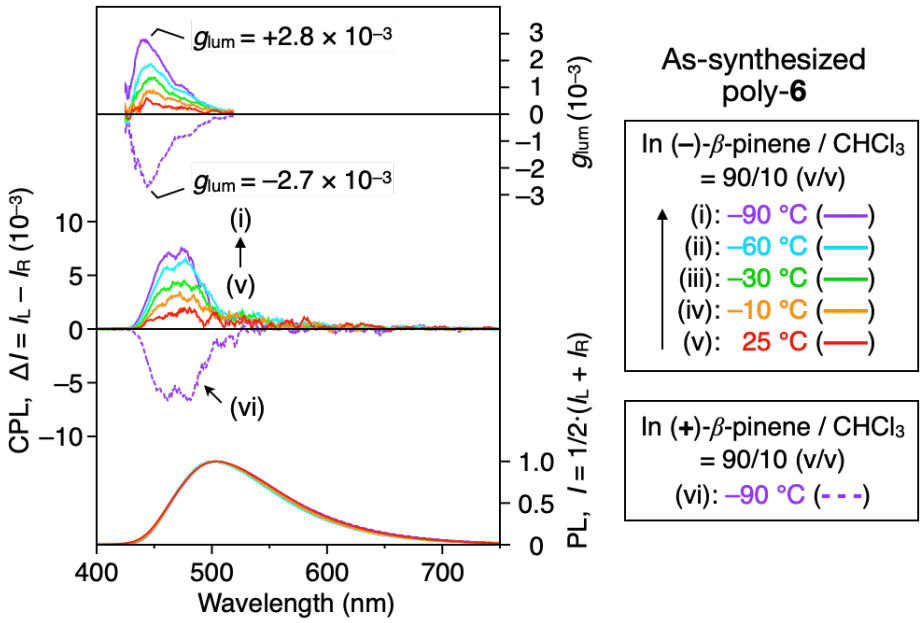


Fig. 6 | CPL induction in poly[4]helicene nanoribbon. Normalized PL (bottom), CPL (middle), and g_{lum} (top) spectra of as-synthesized poly-**6** measured in (–)-*β*-pinene/chloroform (90/10, v/v) at different temperatures (–90 (i), –60 (ii), –30 (iii), –10 (iv), and 25 (v) °C) and in (+)-*β*-pinene/chloroform (90/10, v/v) at –90 °C (vi). λ_{ex} = 300 nm. [Polymer] = 0.15 mM.

Conclusions

We have succeeded in synthesizing a dynamic helical polyhelicene nanoribbon entirely composed of configurationally labile [4]helicene subunits through the quantitative intramolecular alkyne benzannulation of the nonhelical precursor polymer. Both right- and left-handed helical nanoribbons with a poly[4]helicene framework can be induced by a noncovalent interaction with a chiral solvent, mediated by deracemization of the racemic [4]helicene repeating units. Inversion of the helicity of each [4]helicene subunit is mechanically coupled to the helicity of the poly[4]helicene backbone. Hence, deracemization proceeds in a highly-cooperative manner, thus producing a CPL active, right- or left-handed helical poly[4]helicene consisting of homochiral right- or left-handed-[4]helicene subunits, respectively, which can be switched. The present findings have demonstrated that [4]helicene, previously excluded as a structural motif in chiral material construction, can be applied to build a unique polyhelicene framework with a controlled handedness. Furthermore, they will also provide a promising strategy for the development of dynamic and even static one-handed helical polyhelicene nanoribbons, combined with the previously discovered helicity memory technique[50] or by introducing chiral pendants. Work toward these goals is currently underway in our laboratory.

References

1. Ball, M.*, et al.* Contorted polycyclic aromatics. *Acc. Chem. Res.* **48**, 267–276 (2015).
2. Segawa, Y., Ito, H. & Itami, K. Structurally uniform and atomically precise carbon nanostructures. *Nat. Rev. Mater.* **1**, 15002 (2016).
3. Liu, Z.*, et al.* Small size, big impact: Recent progress in bottom-up synthesized nanographenes for optoelectronic and energy applications. *Adv. Sci.* **9**, 2106055 (2022).
4. Izquierdo-García, P., Fernández-García, J. M. & Martín, N. Twenty years of graphene: From pristine to chemically engineered nano-sized flakes. *J. Am. Chem. Soc.* **146**, 32222–32234 (2024).
5. Shen, Y. & Chen, C.-F. Helicenes: Synthesis and applications. *Chem. Rev.* **112**, 1463–1535 (2012).
6. Gingras, M. One hundred years of helicene chemistry. Part 1: Non-stereoselective syntheses of carbohelicenes. *Chem. Soc. Rev.* **42**, 968–1006 (2013).
7. Gingras, M., Félix, G. & Peresutti, R. One hundred years of helicene chemistry. Part 2: Stereoselective syntheses and chiral separations of carbohelicenes. *Chem. Soc. Rev.* **42**, 1007–1050 (2013).
8. Gingras, M. One hundred years of helicene chemistry. Part 3: Applications and properties of carbohelicenes. *Chem. Soc. Rev.* **42**, 1051–1095 (2013).
9. Martin, R. H. & Marchant, M.-J. Thermal racemisation of [6], [7], [8] and [9] helicene. *Tetrahedron Lett.* **13**, 3707–3708 (1972).
10. Ravat, P. Carbo[*n*]helicenes restricted to enantiomerize: An insight into the design process of configurationally stable functional chiral PAHs. *Chem. - Eur. J.* **27**, 3957–3967 (2021).
11. Mori, T. Chiroptical properties of symmetric double, triple, and multiple helicenes. *Chem. Rev.* **121**, 2373–2412 (2021).
12. Kiran, V.*, et al.* Helicenes—A new class of organic spin filter. *Adv. Mater.* **28**, 1957–1962 (2016).
13. Dhbaibi, K., Favereau, L. & Crassous, J. Enantioenriched helicenes and helicenoids containing main-group elements (B, Si, N, P). *Chem. Rev.* **119**, 8846–8953 (2019).

14. Barroso, J., *et al.* Revisiting the racemization mechanism of helicenes. *Chem. Commun.* **54**, 188–191 (2018).
15. Castro Neto, A. H., *et al.* The electronic properties of graphene. *Rev. Mod. Phys.* **81**, 109–162 (2009).
16. Wang, X.-Y., Narita, A. & Müllen, K. Precision synthesis versus bulk-scale fabrication of graphenes. *Nat. Rev. Chem.* **2**, 0100 (2017).
17. Müllen, K. & Scherf, U. Conjugated polymers: Where we come from, where we stand, and where we might go. *Macromol. Chem. Phys.* **224**, 2200337 (2023).
18. Sekhavati, K., Sharma, V. & Keerthi, A. Solution-phase synthesis of graphene nanoribbons: a review on polymerization strategies. *Mater. Adv.* **6**, 4969–4991 (2025).
19. Niu, W., Ma, J. & Feng, X. Precise structural regulation and band-gap engineering of curved graphene nanoribbons. *Acc. Chem. Res.* **55**, 3322–3333 (2022).
20. Fernández-García, J. M., *et al.* Synthetic chiral molecular nanographenes: The key figure of the racemization barrier. *Chem. Commun.* **58**, 2634–2645 (2022).
21. Liu, J., *et al.* Toward cove-edged low band gap graphene nanoribbons. *J. Am. Chem. Soc.* **137**, 6097–6103 (2015).
22. Gu, Y. W., *et al.* Cove-edged nanographenes with localized double bonds. *Angew. Chem., Int. Ed.* **59**, 8113–8117 (2020).
23. Liu, K., *et al.* Cove-edged chiral graphene nanoribbons with chirality-dependent bandgap and carrier mobility. *J. Am. Chem. Soc.* **146**, 1026–1034 (2023).
24. Zhu, X. J., *et al.* Topological structure realized in cove-edged graphene nanoribbons via incorporation of periodic pentagon rings. *J. Am. Chem. Soc.* **146**, 7152–7158 (2024).
25. Daigle, M., *et al.* Helically coiled graphene nanoribbons. *Angew. Chem., Int. Ed.* **56**, 6213–6217 (2017).
26. Yao, X. L., *et al.* Synthesis of nonplanar graphene nanoribbon with fjord edges. *J. Am. Chem. Soc.* **143**, 5654–5658 (2021).
27. Chen, Q., *et al.* Porphyrin-fused graphene nanoribbons. *Nat. Chem.* **16**, 1133–1140 (2024).
28. Dubey, R. K., Melle-Franco, M. & Mateo-Alonso, A. Inducing single-handed helicity in a twisted molecular nanoribbon. *J. Am. Chem. Soc.* **144**, 2765–2774 (2022).

29. Swain, A., Radacki, K., Braunschweig, H. & Ravat, P. Helically twisted nanoribbons *via* stereospecific annulative π-extension reaction employing [7]helicene as a molecular wrench. *Chem. Sci.* **15**, 11737–11747 (2024).
30. Bao, S. T.*, et al.* Chirality unbound in graphene nanoribbons. *Angew. Chem., Int. Ed.* **64**, e202508426 (2025).
31. Xiao, X.*, et al.* Single-handed helicene nanoribbons via transfer of chiral information. *J. Am. Chem. Soc.* **144**, 20214–20220 (2022).
32. Goldfinger, M. B. & Swager, T. M. Fused polycyclic aromatics via electrophile-induced cyclization reactions: Application to the synthesis of graphite ribbons. *J. Am. Chem. Soc.* **116**, 7895–7896 (1994).
33. Ikai, T.*, et al.* Triptycene-based ladder polymers with one-handed helical geometry. *J. Am. Chem. Soc.* **141**, 4696–4703 (2019).
34. Zheng, W., Ikai, T. & Yashima, E. Synthesis of single-handed helical spiro-conjugated ladder polymers through quantitative and chemoselective cyclizations. *Angew. Chem., Int. Ed.* **60**, 11294–11299 (2021).
35. Ikai, T., Oki, K., Yamakawa, S. & Yashima, E. Stereospecific synthesis of enantiopure [6]helicene containing a seven-membered ring and [7]helicene via acid-promoted stepwise alkyne annulations of doubly axial-chiral precursors. *Angew. Chem., Int. Ed.* **62**, e202301836 (2023).
36. Zheng, W., Ikai, T., Oki, K. & Yashima, E. Consecutively-fused single, double, and triple expanded helicenes. *Nat. Sci.* **2**, e20210047 (2022).
37. Zheng, W.*, et al.* One-handed helical tubular ladder polymers for chromatographic enantioseparation. *Angew. Chem., Int. Ed.* **62**, e202218297 (2023).
38. Ikai, T.*, et al.* 2,2′-Tethered binaphthyl-embedded one-handed helical ladder polymers: Impact of the tether length on helical geometry and chiroptical property. *Angew. Chem., Int. Ed.* **63**, e202318712 (2024).
39. Ikai, T.*, et al.* Tunable synthesis of one-handed helical ladder polymers with a helical cavity or helical grooves for advanced chiral recognition. *Macromolecules* **58**, 6943–6952 (2025).

40. Schuster, N. J.*, et al.* A helicene nanoribbon with greatly amplified chirality. *J. Am. Chem. Soc.* **140**, 6235–6239 (2018).
41. Prince, R. B., Barnes, S. A. & Moore, J. S. Foldamer-based molecular recognition. *J. Am. Chem. Soc.* **122**, 2758–2762 (2000).
42. Fujiki, M. Supramolecular chirality: Solvent chirality transfer in molecular chemistry and polymer chemistry. *Symmetry* **6**, 677–703 (2014).
43. Miao, T.*, et al.* Preparation of chiral polymers: Precise chirality transfer from natural species to achiral artificial polymers. *Giant* **14**, 100161 (2023).
44. Yashima, E.*, et al.* Supramolecular helical systems: Helical assemblies of small molecules, foldamers, and polymers with chiral amplification and their functions. *Chem. Rev.* **116**, 13752–13990 (2016).
45. Liu, N., Gao, R.-T. & Wu, Z.-Q. Helix-induced asymmetric self-assembly of π-conjugated block copolymers: From controlled syntheses to distinct properties. *Acc. Chem. Res.* **56**, 2954–2967 (2023).
46. Qiu, Y.*, et al.* Chiral nanostructures from artificial helical polymers: Recent advances in synthesis, regulation, and functions. *ACS Nano* **19**, 229–280 (2025).
47. Wang, H.-X., Zhu, X. & Liu, M. Emergent chiral and topological nanoarchitectonics in self-assembled supramolecular systems. *Chem. Soc. Rev.* **54**, 5516–5550 (2025).
48. Yashima, E.*, et al.* Helical polymers: Synthesis, structures, and functions. *Chem. Rev.* **109**, 6102–6211 (2009).
49. Green, M. M., Khatri, C. & Peterson, N. C. A macromolecular conformational change driven by a minute chiral solvation energy. *J. Am. Chem. Soc.* **115**, 4941–4942 (1993).
50. Shimomura, K.*, et al.* Switchable enantioseparation based on macromolecular memory of a helical polyacetylene in the solid state. *Nat. Chem.* **6**, 429–434 (2014).

Methods

General procedures for the synthesis of the precursor polymers. Poly-**5** and poly-**5**-8.9K were prepared by Suzuki−Miyaura coupling copolymerizations of $\mathbf{Ph_{Br}}$ with $\mathbf{NAP_{Bpin}}$ in a dry Schlenk flask under a dry nitrogen atmosphere (Supplementary Scheme 2). The results of the copolymerizations are summarized in Supplementary Table 1. A typical polymerization procedure is described below.

$\mathbf{Ph_{Br}}$ (200 mg, 0.257 mmol), $\mathbf{NAP_{Bpin}}$ (262 mg, 0.263 mmol), and tripotassium phosphate (336 mg, 1.58 mmol) were placed in a dry Schlenk flask, which was then evacuated on a vacuum line and flushed with dry nitrogen. After this evacuation-flush procedure was repeated three times, a degassed tetrahydrofuran (THF)/water mixture (2/1, v/v; 3.0 mL) was added using a syringe. To this was added chloro[(tri-*tert*-butylphosphine)-2-(2-aminobiphenyl)]palladium(II) (P(*t*-Bu)$_3$ Pd G2) (13.7 mg, 26.8 μmol) and the mixture was stirred at room temperature for 18 h. After THF was added to the reaction mixture, the resulting polymer was precipitated into a large amount of methanol and collected by centrifugation. After washing with methanol and drying in vacuo at room temperature (178 mg, 93% yield), the obtained poly-**5** (150 mg) was subjected to preparative SEC using a Tosoh TSKgel GMHXL (30 cm × 21.5 mm (i.d.)) to remove oligomers (59 mg, 37% yield) (entry 1 in Supplementary Table 1). In the same way, poly-**5**-8.9K with a lower M_n value was prepared with a shorter reaction time (5 min) (entry 2). The M_n and M_w/M_n values of the random-coil precursors were estimated by SEC using polystyrene standards in chloroform.

General procedures for alkyne benzannulation of the precursor polymers. Poly-**6** and poly-**6**-8.5K were prepared by alkyne benzannulations of the corresponding precursor polymers (poly-**5** and poly-**5**-8.9K, respectively) with TFA in a dry Schlenk flask under a dry nitrogen atmosphere in a similar way as previously reported (Fig. 3a and Supplementary Scheme 3).[34] A typical procedure for the alkyne benzannulation is described below.

The precursor polymer poly-**5** (6.2 mg, 33.8 μmol) was placed in a dry Schlenk flask, which was then evacuated on a vacuum line and flushed with dry nitrogen. After this evacuation-flush procedure was repeated three times, an anhydrous dichloromethane/TFA mixture (60/1, v/v; 1 mL) was added at room temperature using a syringe. After 22 h, the reaction mixture was diluted with chloroform, the solution was washed with saturated aqueous $NaHCO_3$ and water, and then dried over Na_2SO_4. After

filtration, most of the solvent was removed under reduced pressure and the concentrated solution was poured into a large amount of methanol. The resulting polymer was collected by centrifugation, washed with methanol, and dried in vacuo to yield poly-**6** (6.0 mg, 97% yield). In the same way, poly-**6**-8.5K was prepared from its precursor poly-**5**-8.9K (Supplementary Scheme 3). The M_n and M_w/M_n values of the poly[4]helicenes were estimated by SEC using polystyrene standards in chloroform.

Data availability

Data supporting the findings of this study are available in the article and Supplementary Information files, or from the corresponding author upon request.

Acknowledgements

We thank Mr. Kanta Wakabayashi (Nagoya University) for his assistance in the spectral measurements. This work was supported in part by JSPS KAKENHI (Grant-in-Aid for Specially Promoted Research, no. 18H05209 (E.Y. and T.I.), Grant-in-Aid for Scientific Research (B), no. 24K01537 (T.I.), and Grant-in-Aid for Challenging Research (Exploratory) (no. 23K17939 (T.I.)) and JST PRESTO (no. JPMJPR21A1 (T.I.)). T.I. gratefully acknowledges the Mitsubishi Foundation and Toshiaki Ogasawara Memorial Foundation for financial support.

Author contributions

T.I. conceived the idea, directed the project, and designed the experiments. E.Y. designed the experiments, directed the project, and supervised the research. H.I., K.O., and M.Y. performed the experiments. J.P. and Y.H. performed MD simulations. T.I. and E.Y. co-wrote the manuscript with contributions from all authors.

Competing interests

The authors declare no competing interests.

Additional information

The online version contains supplementary material available at https://doi.org/10.1038/XXX.

Figure legends

Fig. 1 | Development of a dynamic helical poly[4]helicene nanoribbon composed of configurationally labile [4]helicene subunits. a, Representative examples of the partial structures of the cove- and fjord-edged graphene nanoribbons (GNRs) incorporating the [4]- and [5]helicene subunits at the graphene periphery, respectively. **b**, Structures of a one-handed helical ladder polymer (poly-(*S*)-**A**) and a fully π-conjugated coplanar ladder polymer (poly-**B**). **c**, Structure of a dynamic helical poly[4]helicene nanoribbon (poly-**6**) composed entirely of configurationally labile [4]helicene subunits. **d**, Schematic illustrations of cooperative one-handed helicity induction in the poly[4]helicene nanoribbon mediated by deracemization of the dynamically racemic [4]helicene repeating units through supramolecular chirality transfer from optically-active natural solvents ((–)- and (+)-*β*-pinene), resulting in circularly polarized luminescence (CPL) capable of switching the polarization handedness (left (*l*) and right (*r*)).

Fig. 2 | Quantitative and chemoselective synthesis of consecutively fused multiple [4]helicenes. a, Synthesis of consecutively fused multiple [4]helicenes (double-**2** and quadruple-**4**) through quantitative and chemoselective acid-promoted alkyne benzannulations of **1** and **3**, respectively. **b**, ^{1}H NMR spectra (500 MHz, $CDCl_3$, 25 °C) of **1** (i), **3** (iii), and as-synthesized cyclization products (double-**2** (ii) and quadruple-**4** (iv)) obtained from **1** and **3**, respectively. For the signal assignments and the corresponding IR spectra, see Supplementary Figs. 5, 7, and 8. **c**, X-ray crystal structure of double-**2**. **d**, Crystal packing structure of (*M*,*M*)/(*P*,*P*)-double-**2** as viewed along the *b* axis of the unit cell shown in gray. The helicene backbones and the 4-butoxy-2,6-dimethylphenyl pendant groups are represented by capped-stick and wireframe models, respectively, and (*M*,*M*)- and (*P*,*P*)-double-**2** are colored in red and blue, respectively. All the hydrogen atoms are omitted for clarity.

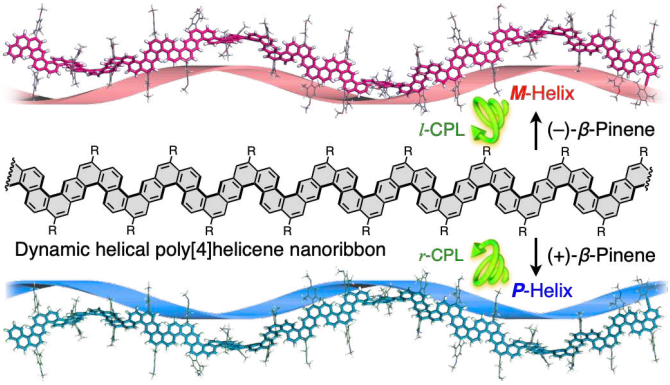
Fig. 3 | Defect-free synthesis of poly[4]helicene nanoribbon. a, Synthesis of a dynamic helical poly[4]helicene nanoribbon (poly-**6**) by quantitative and chemoselective acid-promoted alkyne benzannulations of poly-**5**. **b**, ^{1}H NMR spectra (500 MHz, 1,1,2,2-tetrachloroethane-d_2, 95 °C) of poly-**5** (i) and poly-**6** (ii). For the corresponding IR spectra, the variable-temperature ^{1}H NMR spectra, and the signal assignments, see Supplementary Figs. 8 and 10–13. Asterisks in (i) denote the aromatic protons from alkoxyphenyl pendants (R^2) at the terminal end (Supplementary Figs. 14 and 15). **c**, Absorption (solid lines) and normalized PL (dotted lines) spectra of double-**2** (i,iv), quadruple-**4** (ii,v), and poly-**6** (iii,vi) in chloroform at 25 °C (i–iii) and room temperature (iv–vi). [**2**, **4**, or poly-**6**] = 0.15 mM. **d**, Photographs of double-**2** (i), quadruple-**4** (ii), and poly-**6** (iii) in chloroform with 365-nm irradiation. Fluorescence quantum yields (Φ_F) are also shown.

Fig. 4 | Computational structural analysis of poly[4]helicene nanoribbon. a, Side views of hexadeca-**6**-H (16-mer model of poly-**6** without aryl pendants) containing 32 [4]helicene units before (i) and after (ii) the molecular dynamics (MD) simulation at 20 °C (293 K) for 60 ns. The structures are represented by capped-stick models, and the carbon atoms of the (*P*)- and (*M*)-[4]helicene units in the backbone are highlighted in blue and red, respectively, for clarity. **b**, Relative free energies (kJ/mol) for tetra-**6** (4-mer model of poly-**6**) containing 8 [4]helicene units calculated by density functional theory (DFT) at the B3LYP/6-31G(d) level. For simplicity, the branched alkoxy pendants are replaced with methoxy groups.

Fig. 5 | Cooperative one-handed helicity induction in poly[4]helicene nanoribbon. a, CD and absorption spectra of as-synthesized poly-**6** in (–)-*β*-pinene/chloroform (90/10, v/v) at different temperatures (–90 (i), –80 (ii), –60 (iii), –30 (iv), –10 (v), and 25 (vi) °C) and in (+)-*β*-pinene/chloroform (90/10, v/v) at –90 °C (vii). [Polymer] = 0.15 mM. **b**, Plots of Kuhn's dissymmetry factors ($|g_{abs}|$) at the maximum Cotton effect of fractionated poly-**6**, quadruple-**4**, and double-**2** versus the M_n (for poly-**6**) or molecular weights (MW) (for quadruple-**4** and double-**2**) value. For the SEC fractionation of as-synthesized poly-**6** and poly-**6**-8.5K and the corresponding CD spectra, see Supplementary Fig. 25. **c**, Top (left) and side (right) views of the geometry-optimized structures of the (*M*)-handed helical poly-**6** composed entirely of (*M*)-[4]helicene units with 16 repeating units obtained by the molecular mechanics (MM) calculations (Compass II force field). For simplicity, all alkoxy pendants are replaced with methoxy groups. The structures of the helical ladder backbones and alkoxyphenyl pendants are represented by capped-stick and wireframe models, respectively, and the carbon atoms of the helical ladder backbones are highlighted in red for clarity.

Fig. 6 | CPL induction in poly[4]helicene nanoribbon. Normalized PL (bottom), CPL (middle), and g_{lum} (top) spectra of as-synthesized poly-**6** measured in (–)-*β*-pinene/chloroform (90/10, v/v) at different temperatures (–90 (i), –60 (ii), –30 (iii), –10 (iv), and 25 (v) °C) and in (+)-*β*-pinene/chloroform (90/10, v/v) at –90 °C (vi). λ_{ex} = 300 nm. [Polymer] = 0.15 mM.

Graphical abstract



Supplementary Files

This is a list of supplementary files associated with this preprint. Click to download.

- double2.cif
- checkcifdouble2.pdf
- IkaiSI.pdf
- SupplementaryVideo1.mp4
- SupplementaryVideo2.mp4